Magnetic ground state of the ordered double-perovskite Sr_2YbRuO_6: Two magnetic transitions

Shivani Sharma,[1,2,*] D. T. Adroja,[1,3,†] C. Ritter,[4] D. Khalyavin,[1] P. Manuel,[1] Gavin B. G. Stenning,[1] A. Sundaresan,[2] A. D. Hillier,[1] P. P. Deen,[5,6] D. I. Khomskii,[7] and S. Langridge[1]

[1]*ISIS facility, Rutherford Appleton Laboratory, Chilton Oxon OX11 0QX, United Kingdom*

[2]*School of Advanced Materials, Chemistry and Physics of Materials Unit, Jawaharlal Nehru Centre for Advanced Scientific Research, Jakkur, Bangalore 560 064, India*

[3]*Highly Correlated Matter Research Group, Physics Department, University of Johannesburg, Auckland Park 2006, South Africa*

[4]*Institut Laue-Langevin, 71 Avenue des Martyrs, CS 20156, 38042, Grenoble Cedex 9, France*

[5]*European Spallation Source ERIC, 22363 Lund, Sweden*

[6]*Niels Bohr Institute, University of Copenhagen, 2100 Copenhagen, Denmark*

[7]*II Physikalisches Institut, Universitaet zu Koeln, Zuelpicher Strasse 77, 50937 Koeln, Germany*

(Received 25 February 2020; revised 10 September 2020; accepted 11 September 2020; published 9 October 2020)

Comprehensive muon-spin-rotation/relaxation (μSR) and neutron powder-diffraction (NPD) studies supported via bulk measurements have been performed on the ordered double-perovskite Sr_2YbRuO_6 to investigate the nature of the magnetic ground state. Two sharp transitions at $T_{N1} \sim 42$ K and $T_{N2} \sim 36$ K have been observed in the static and dynamic magnetization measurements, coinciding with the heat-capacity data. In order to confirm the origin of the observed phase transitions and the magnetic ground state, microscopic evidences are presented here. An initial indication of long-range magnetic ordering comes from a sharp drop in the muon initial asymmetry and a peak in the relaxation rate near T_{N1}. NPD confirms that the magnetic ground state of Sr_2YbRuO_6 consists of an antiferromagnetic (AFM) structure with interpenetrating lattices of parallel Yb^{3+} and Ru^{5+} moments lying in the *ab* plane and adopting an *A*-type AFM structure. Intriguingly, a small but remarkable change is observed in the long-range ordering parameters at T_{N2} confirming the presence of a weak spin reorientation (i.e., change in spin configuration) transition of Ru and Yb moments, as well as a change in the magnetic moment evolution of the Yb^{3+} spins at T_{N2}. The temperature-dependent behavior of the Yb^{3+} and Ru^{5+} moments suggests that the 4*d* electrons of Ru^{5+} play a dominating role in stabilizing the long-range-ordered magnetic ground state in the double-perovskite Sr_2YbRuO_6 whereas only the Yb^{3+} moments show an arrest at T_{N2}. The observed magnetic structure and the presence of a ferromagnetic interaction between Ru and Yb ions are explained with use of the Goodenough-Kanamori-Anderson rules. Possible reasons for the presence of the second magnetic phase transition and of a compensation point in the magnetization data are linked to competing mechanisms of magnetic anisotropy.

DOI: 10.1103/PhysRevB.102.134412

I. INTRODUCTION

Mixed ruthenates with perovskite-based crystal structures have been receiving considerable attention in recent decades [1–8], because of their interesting magnetic properties including the recent discovery of spin-triplet superconductivity in the layered ruthenate Sr_2RuO_4 [9]. Despite the rarity of 4*d*-based magnetic materials, $SrRuO_3$ has a robust Curie temperature $T_C \sim 165$ K with saturation magnetization value of 1.4 μ_B/Ru and a metallic ground state [10], while $SrRu_2O_6$ exhibits antiferromagnetic (AFM) ordering at $T_N = 563$ K and has a semiconducting ground state [11]. Sr_2YRuO_6, which has essentially the same crystal structure as $SrRuO_3$, but with every second Ru substituted by Y, orders in an AFM structure with an insulating ground state [1,3]. Interestingly the estimates of the ordered Ru moments is even higher than those of the parent compound, although the critical temperature is strongly reduced to 32 K (T_{N1}) with a second AFM transition $T_{N2} = 24$ K [1,3].

A detailed study of the M_2RERuO_6 (M = Ca, RE = Y, La, or Eu; M = Sr, RE = Y; M = Ba, RE = La or Eu) ruthenium perovskites was carried out by Greatrex *et al.* [12], who determined the crystal structure, and measured the temperature dependence of the electrical resistivity, the magnetic susceptibility, and the ^{99}Ru Mössbauer effect at 4.2 K. They reported that these materials crystallize in the monoclinic $P2_1/n$ space group and are magnetically ordered at 4.2 K, with T_N ranging from 12 K for Ca_2LaRuO_6 to <80 K for Ba_2LaRuO_6, with hyperfine magnetic fields B_{hf} at the Ru sites between 56 and 60 T due to the electronic magnetic ordering [12]. In subsequent years, the AFM ordered Ru-based double-perovskites Sr_2RERuO_6 (RE = rare-earth Ho, Tb, Yb, Dy, and Lu or Y, etc.) were reported to exhibit two magnetic transitions and strong geometrical frustration above the magnetic ordering for some of these systems confirmed via bulk and microscopic measurements [3–6,8]. Recent

*phy.shivanisharma@gmail.com
†devashibhai.adroja@stfc.ac.uk

neutron-diffraction studies for $RE = Y$ allowed us to understand and differentiate the origin of the two magnetic transitions [3] whereas for $RE =$ Dy, Ho, and Tb, the difference between the two magnetic transitions could not be resolved in the neutron-diffraction study within the available instrumental resolution [5,8]. In Sr_2YRuO_6, only half of the Ru layers order magnetically below T_{N1} while the other half (alternately) reveals short-range ordering. Furthermore, below T_{N2}, the system exhibits a fully ordered type-I AFM ground state [3]. The cubic double-perovskite Ba_2YRuO_6 with space group Fm-$3m$ also exhibits two apparent transitions at 47 and 36 K and type-I AFM ground state at low temperature [13]. Polarized neutron-diffraction data revealed that this regime between 36 and 47 K is dominated by short-range spin correlations. However, the origin of T_{N2} in some of these double perovskites with type-I AFM structure below T_{N1} is still an open question [4,5,14,15] and the aim of the present work is to develop better understanding using the experimental data which could help to resolve this enigma for Sr_2YbRuO_6.

Earlier assumptions that the two magnetic transitions in Sr_2YbRuO_6 are due to the ordering of Yb and Ru moments at different temperatures seem unlikely due to the presence of two such transitions in the Sr_2YRuO_6 where only one magnetic cation (i.e., Ru) is present [3,4]. Further intriguing facts regarding the magnetic ground state of the Ru- based double perovskites are the similar ordered moment values ($\sim 2\mu_B$) found for the Ru^{5+} ion irrespective of the nature of the RE (rare-earth) atom and the small value of the ordered moments of the magnetic RE ions [3,5,8]. All these results motivate further exploration of the other members of this family in order to understand the origin of the two magnetic transitions, the role of the Ru atom in the magnetic ordering, and the participation of rare-earth atom in determining the magnetic ground state.

Sr_2YbRuO_6 is a magnetic insulator with a double-perovskite structure, which undergoes a long-range magnetic ordering transition below T_{N1} (42 K), in addition to the conspicuous occurrence of the second transition at $T_{N2} = 36$ K and a weak anomaly at $T^* = 10$ K [4,15]. Sr_2YbRuO_6 also displays a temperature induced magnetization reversal almost coinciding with T_{N2} due to an underlying magnetic compensation phenomenon [16]. The observed magnetic entropy $S_{mag} = 5.7\,J\,mol^{-1}\,K^{-1}$ at 60 K is smaller than the expected value for ordered Ru^{5+} moments with a ground state of $J = 3/2$ ($S_{mag} = 11.52\,J\,mol^{-1}\,K^{-1}$) [4]. This was tentatively linked to the presence of frustration above the magnetic transition. The same group has also reported the exchange bias effect in Sr_2YbRuO_6 below the compensation temperature [16]. The compensation temperature was referred to as the temperature where the measured magnetization becomes zero [4] and a crossover of zero-field-cooled and field-cooled magnetization occurs. However, in the same report, it was suggested that two magnetic anomalies near T_{N1} and T_{N2} could be due to the magnetic ordering of Ru^{5+} ($4d$ [3]) and Yb^{3+} ($4f$ [13]) moments, respectively. Later, Doi *et al.* [15] reported a type-I AFM structure below T_{N1} confirmed via neutron powder-diffraction (NPD) study performed at 10 K. However, due to the lack of systematic temperature-dependent NPD data, no information is available regarding the thermal evolution of the magnetic structure at T_{N2} [14,15]. Here, we present a detailed NPD and μSR study, which, supported by exhaustive magnetization and heat capacity data, confirms that both the Ru^{5+} and Yb^{3+} moments order at T_{N1} and that a weak spin reorientation takes place at T_{N2}. We use this term "spin reorientation" in the sense of "change in the relative spin configuration." No change or anomaly has been found near $T^* \sim 10$ K in the NPD data.

II. EXPERIMENTAL DETAILS

The polycrystalline sample of Sr_2YbRuO_6 was prepared by the standard solid-state reaction using the same protocol as mentioned elsewhere [4]. Phase purity was confirmed by x-ray diffraction (XRD) using a Rigaku Smartlab x-ray diffractometer equipped with a Ge two bounce monochromator enabling Cu-$K\alpha$ radiation. The dc magnetization measurements have been performed on a Quantum Design's superconducting quantum interference device magnetometer. Temperature-dependent heat capacity, using a relaxation technique, and ac susceptibility were measured using a PPMS by Quantum Design. To investigate the magnetic structure/ground state, temperature-dependent NPD measurements were carried out using the time-of-flight diffractometer WISH at the ISIS Facility, UK [17]. The FULLPROF_Suite has been used to analyze the XRD and NPD data [18]. The MuSR spectrometer in longitudinal geometry at the ISIS Pulsed Neutron and Muon Source, UK, has been employed to carry out zero-field (ZF) muon-spin-rotation/relaxation (μSR) experiments. The powder sample was mounted onto a silver plate (99.999% purity) using GE varnish and was covered with thin silver foil. The μSR measurements were carried out using a He [4] cryostat between 2 and 300 K.

III. RESULTS AND DISCUSSION

A. X-ray diffraction

The room-temperature XRD pattern of Sr_2YbRuO_6 has been Rietveld refined using monoclinic symmetry (space group $P2_1/n$) with an ordered arrangement of Yb^{3+} and Ru^{5+} atoms at the B site. The result is shown in Fig. 1(a) and is in good agreement with the existing literature [4,14]. No extra peaks were evident in the XRD pattern while a very minute impurity phase of Yb_2O_3 was evident in the NPD pattern. One can easily miss this minute impurity with a lab source based XRD machine, while with the high intensity availability of the neutron beam on the WISH instrument, this minute phase can be easily seen. The results of NPD will be discussed in later sections. It is imperative to mention that the magnetic ordering of the impurity phase Yb_2O_3 cannot be responsible for the appearance of T^* as its transition temperature is much lower at about 2.25 K [19]. The crystal structure and the details of Sr_2YbRuO_6 are presented in Fig. 1(b). Bond lengths and bond angles governing the different magnetic interaction pathways are shown in the enlarged views of two dashed box regions, Figs. 1(c) and 1(d).

B. ac and dc Magnetization

Figure 2(a) displays the zero-field-cooled (ZFC) and field-cooled (FC) dc magnetization (χ_{dc}) behavior of Sr_2YbRuO_6

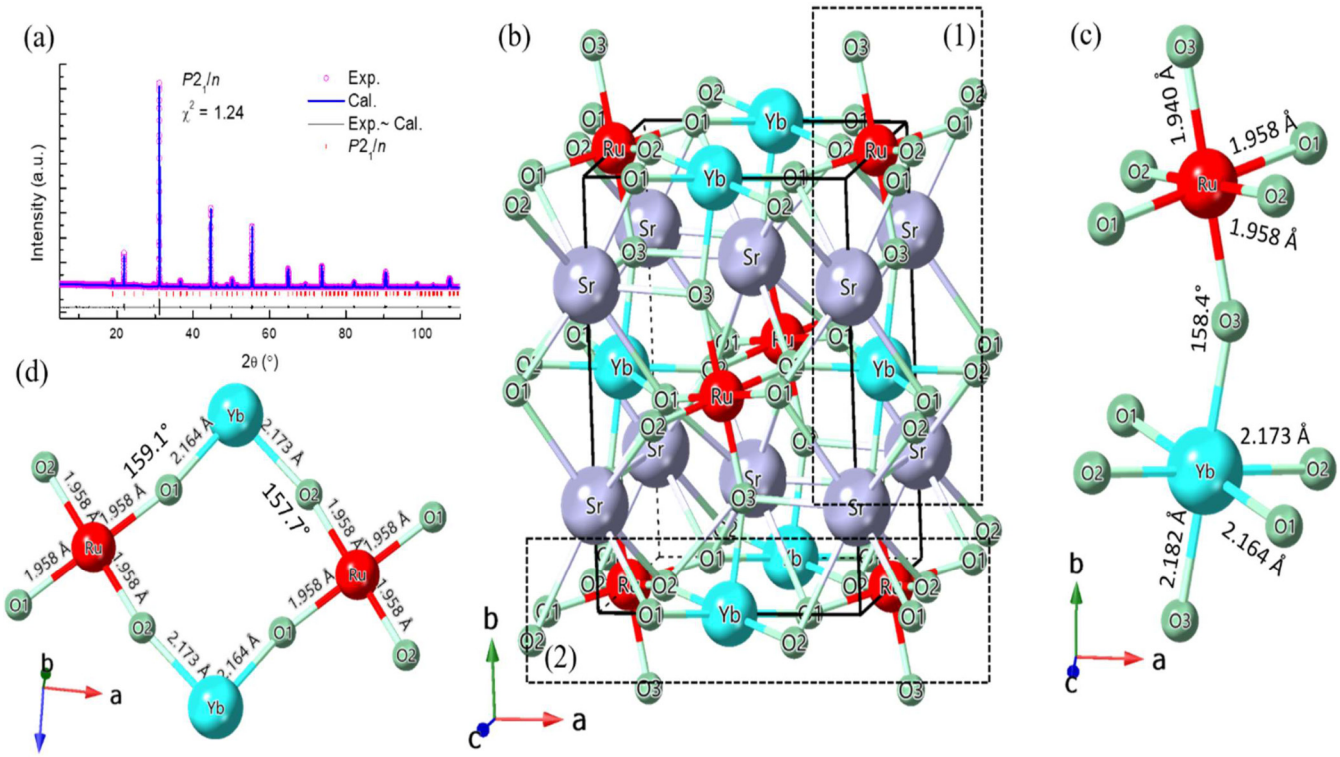

FIG. 1. (a) Rietveld refined XRD pattern of Sr_2YbRuO_6 at 300 K using the monoclinic space group $P112_1/n$. (b) Schematic representation of crystal structure at room temperature. The enlarged view of two dashed box regions is given in (c) and (d) respectively to clearly show the various bond lengths and bond angles in order to explain the possible magnetic interactions pathways. The local point symmetry of both Ru and Yb ion is triclinic (C_i) in the monoclinic crystal structure.

measured in different fields namely, at 50 Oe, 100 Oe, and 10 kOe as a function of temperature. The bifurcation of the ZFC and FC magnetization only starts below a certain critical temperature, followed by a crossover between the ZFC and FC curve. For low applied fields (50 and 100 Oe), the FC magnetization becomes negative by cooling the sample below the crossover point, whereas for sufficiently high fields (10 kOe), the FC curve stays always positive. Noticeably, the ZFC magnetization decreases below 42 K showing a plateau for a small temperature region down to 36 K. Below 36 K the ZFC, magnetization increases with decreasing temperature, irrespective of the applied field value. Here we denote these anomalies by T_{N1} (42 K) and T_{N2} (36 K), respectively. The justification and microscopic evidence to denote them as AFM ordering temperatures (T_N's) comes from the NPD results which are discussed later. Another intriguing feature is the presence of a weak anomaly near 10 K. A similar anomaly below 15 K was previously mentioned to exist by Singh *et al.* [4]. We denote this anomaly by T^*, as we do not have any existing information about its origin. Both the ZFC and FC curves exhibit a small kink near T^*.

To investigate further the nature of these magnetic anomalies, isothermal magnetization has been measured at selected temperatures. Figure 2(b) represents the magnetic isotherms measured at $T = 5$, 30, 37, 50, and 300 K. Noticeably, a weak hysteresis starts to develop below 37 K and becomes quite prominent for the 5 and 30 K curves. It suggests the contribution of a minor ferromagnetic (FM) component to the dominant AFM ground state. The 300 and 50 K curves exhibit a linear behavior, as expected for a paramagnetic state.

To understand the dynamic response of these anomalies, the ac susceptibility (χ_{ac}) of Sr_2YbRuO_6 has been measured. Figure 3 represents the real (χ') part of χ_{ac} as a function of temperature measured at different frequencies. Two clear anomalies are visible in the χ' behavior near T_{N1} and T_{N2}. The frequency-independent behavior of the first anomaly at T_{N1} indicates the onset of long-range ordering below T_{N1} as shown in the enlarged view as inset (i) of Fig. 3. A weak frequency dispersion can be seen below T_{N2}, which indicates the change in magnetic interactions at this point, shown in inset (ii) of Fig. 3. A similar kind of frequency dispersion at T_N has also been observed for other systems showing the long-range ordered state, for example Sr_3NiIrO_6 and Sr_2DyRuO_6 (near T_{N2}) [8,20,21]. A very weak, indirect but apparent signature of a third anomaly near T^* can be seen in the χ_{ac} behavior at $T = 10$ K. The frequency dispersion decreases below T^* and χ' increases sharply. The direct signatures of T_{N1} and T_{N2} have been also found in the χ'' behavior but due to the weak signal, it is difficult to find any signature of T^* in χ'' behavior (data are not shown here).

C. Heat capacity

The heat capacity of Sr_2YbRuO_6 measured in 0 and 2 T applied field is presented in Fig. 4. Two clear peaks are visible near 42 and 36 K, coinciding with the magnetic anomalies at T_{N1} and T_{N2}, respectively, which confirms the long-range

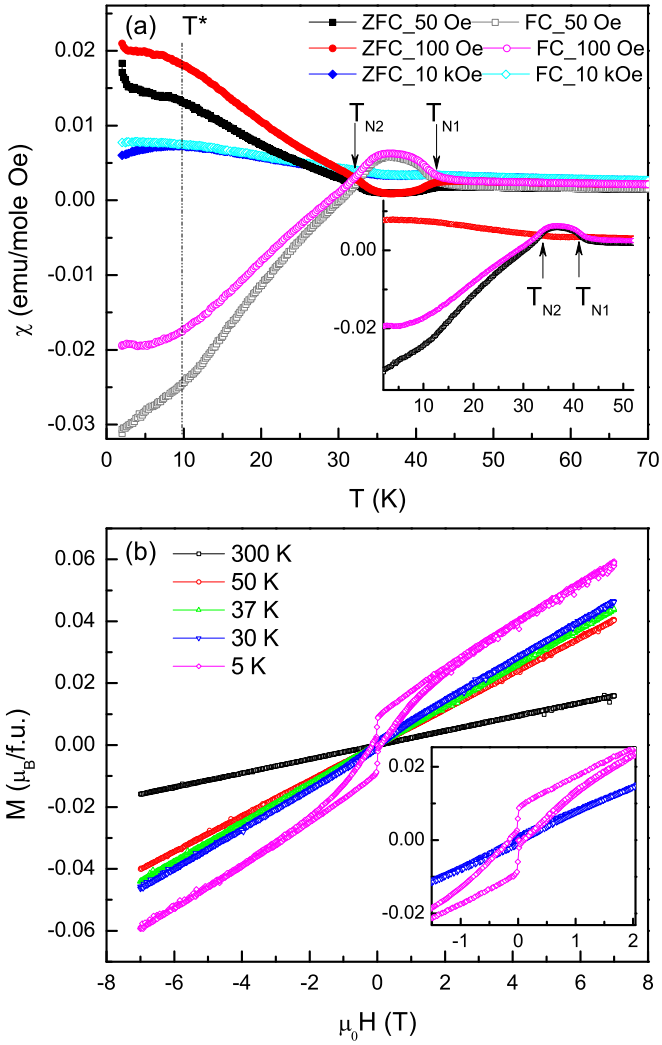

FIG. 2. (a) The dc magnetic susceptibility (χ_{dc}) measured at various applied magnetic fields in zero-field-cooled (ZFC) and field-cooled (FC) conditions. The arrows indicate the magnetic transitions as T_{N1} and T_{N2} and the dashed line indicates the third weak anomaly T^* near 10 K. The inset shows the enlarged view close to magnetic transitions. (b) Magnetization isotherms measured at various temperatures ranging from 5 to 300 K. The inset shows the enlarged view at lower fields data to show the hysteresis observed at 5 and 30 K.

ordering at these transitions. However, no feature or anomaly has been observed near T^*. Also, there is no appreciable change in the heat capacity behavior measured with 0 and 2 T applied field (Fig. 4). Therefore, the static and dynamic magnetization and heat capacity measurements confirm the presence of two long-range transitions at T_{N1} and T_{N2}.

D. Muon spin rotation and relaxation

In order to understand the microscopic origin and local magnetic response of different phase transitions as observed through the bulk techniques, the zero field (ZF) μSR spectra of Sr_2YbRuO_6 have been recorded at various temperatures between 2 and 90 K as shown in Fig. 5. The spectra at 90 and 50 K exhibit weak relaxation and have the same initial asymmetry. However, below 45 K, the relaxation rate increases

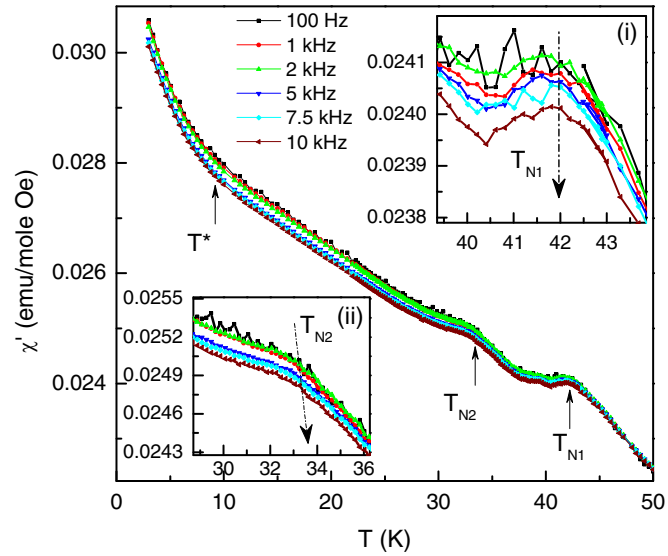

FIG. 3. Real part of ac susceptibility (χ') measured with 10-Oe drive field in zero-field-cooled conditions at different frequencies ranging from 100 Hz to 10 kHz. The arrows indicate the magnetic transitions temperatures, T_{N1} and T_{N2}. The insets (i) and (ii) represent the enlarged view near T_{N1} and T_{N2} respectively. The peak at T_{N1} is frequency independent while the feature at T_{N2} is slightly frequency dependent. Refer to text for details.

faster and the initial asymmetry decreases with decreasing temperature. This is a typical behavior observed near a long-range magnetic ordering transition. The ZF μSR data are fitted using an exponential function with a constant background,

$$G_z(t) = A_0 \exp(-\lambda t) + A_{bg}. \quad (1)$$

Here A_0 is the muon initial asymmetry, λ is the muon relaxation rate, A_{bg} is the constant background arising from muons stopping on the sample holder. The value of $A_{bg} = 0.02$ was estimated from the fitting of the 90-K data and then kept fixed for fitting the data at other temperatures. The fitting

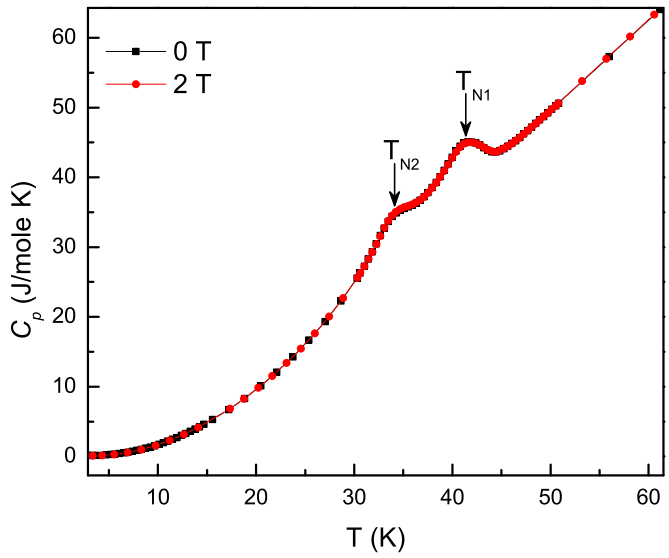

FIG. 4. Heat capacity as a function of temperature in zero and 2 T applied magnetic field.

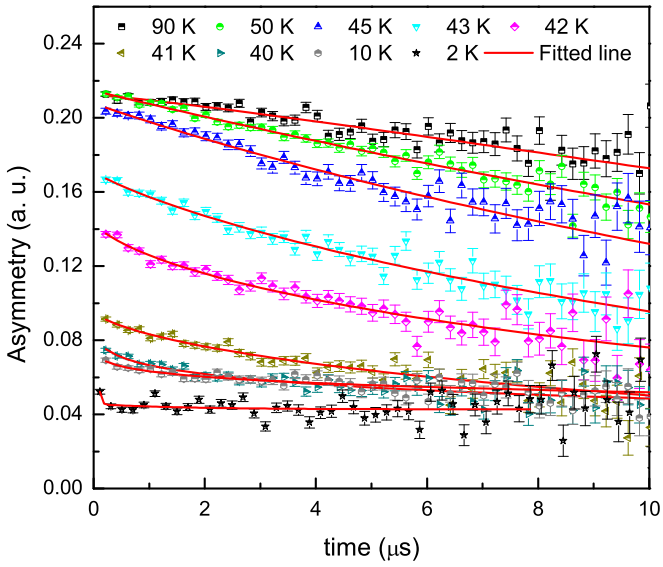

FIG. 5. Zero-field μSR spectra measured at various temperatures. The experimental data are shown by the symbols and the solid red line shows fit to the data using an exponential decay function.

parameters, relaxation rate (λ), and initial asymmetry (A_0) are plotted in Fig. 6. For temperatures down to 50 K, the initial asymmetry is almost temperature independent, which can be attributed to fluctuations of the paramagnetic moments of the Yb^{3+} and Ru^{5+} ions. $\lambda(T)$ increases below 50 K and exhibits a sharp maximum near 42 K (T_{N1}). At T_{N1}, the initial asymmetry drops down by more than 2/3 of the initial value, which indicates that the magnetic ordering is bulk in nature. In a polycrystalline sample, below the magnetic ordering temperature, muons see three components (one longitudinal and two transverse) of the internal field at muon stopping sites. For a bulk magnetic ordering with larger magnetic moments one expects a 2/3 loss of initial asymmetry (the 2/3 transverse component gives oscillations and the 1/3 longitudinal component gives a relaxation) as the transverse component can be seen only very close to the zero-time limit for larger internal fields at muon stopping sites. In the present case, the asymmetry loss is slightly larger than 2/3, which could be due to a fast relaxing component below T_{N1} at smaller time, which cannot be estimated due to the muon pulse width (70 ns full width at half maximum) at ISIS. For $T < T_{N1}$, the further loss in initial asymmetry is very small while the relaxation rate $\lambda(T)$, after peaking at T_{N1}, continues to decrease down to lowest temperatures. As expected A_0 does not reveal any sign of a second/third transition as the system is in a complete long-range magnetic order state below T_{N1} and hence cannot lose further asymmetry. It is interesting to notice that the observed maxima/peak in $\lambda(T)$ near T_{N1} agrees with the susceptibility and heat capacity data. However, the continuous change of $\lambda(T)$ across T_{N2} and T^* indicates a small change in the magnetic structure specifically at T_{N2}. Similar kinds of responses have been recently observed for various other perovskites [7,22–25] and have been helpful in exploring the magnetic ground states, including the microscopic coexistence of magnetic ordered and nonmagnetic phases in $Ba_2PrRu_{0.9}Ir_{0.1}O_6$ using μSR [26].

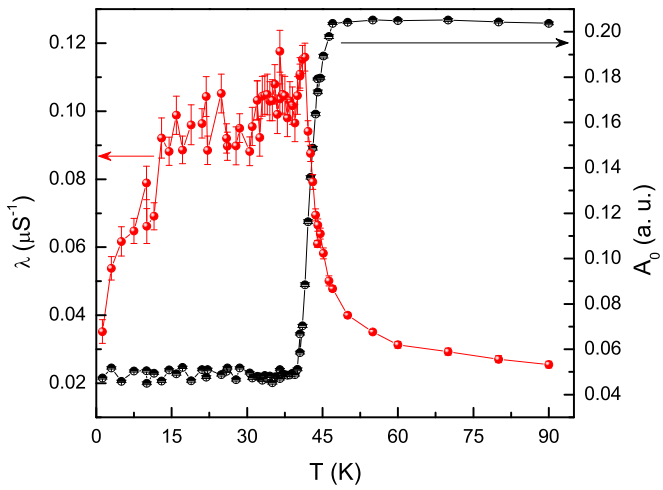

FIG. 6. The temperature-dependent parameters obtained from the fit to μSR spectra as a function of temperature. The initial muon asymmetry (A_0) and relaxation rate (λ) are plotted on right and left y scale with linked x scale.

E. Neutron diffraction

To investigate the magnetic ground state and the possible changes in the magnetic structure across the different transitions, NPD data have been collected on the WISH time-of-flight diffractometer at several temperatures between 100 and 2 K with close data points between 45 and 2 K. The emergence of new peaks along with the enhancement in the intensity of some nuclear peaks is clearly observed below T_{N1}. Figure 7 represents in a 3D plot the thermodiffractogram of Sr_2YbRuO_6 for $T < 45$ K and interplanar spacing $d > 3.5$ Å. All the magnetic reflections can be indexed with a propagation vector $k = (0, 0, 0)$. The occurrence of the (010) reflection indicates that the magnetic moments should have components perpendicular to the b direction. No additional magnetic Bragg peaks appear below T_{N2} or below T^*. The black and red arrows in Fig. 7 point to the temperatures corresponding to T_{N1} and T_{N2}. A nonmonotonic change of the intensities of the magnetic Bragg peaks is visible at T_{N2} and suggests a change in the magnetic structure across T_{N2}. However, a detailed Rietveld refinement is needed to confirm and describe these changes of the magnetic structure at T_{N2}; this will be discussed below. A qualitative representation is given in Fig. 8 where the thermal evolution of the integrated intensity of various magnetic reflections is plotted against temperature. All reflections exhibit a first rise below T_{N1} concomitant with the onset of long-range ordering. Below T_{N2}, they exhibit a more or less pronounced accelerated enhancement in the diffracted intensity with decreasing temperature. Since all the observed magnetic Bragg peaks can be fitted with the type-I AFM structure (which is discussed below in detail), the observation of two different temperature regions in the thermal behavior of the magnetic reflections can explain the existence of two peaks in the magnetization and the heat capacity behavior. The red lines in Fig. 8 are guides to the eye for the expected temperature variation of moment components arising below T_{N1} and T_{N2}. The temperature evolution of (010) and (100/001) peaks in Fig. 8

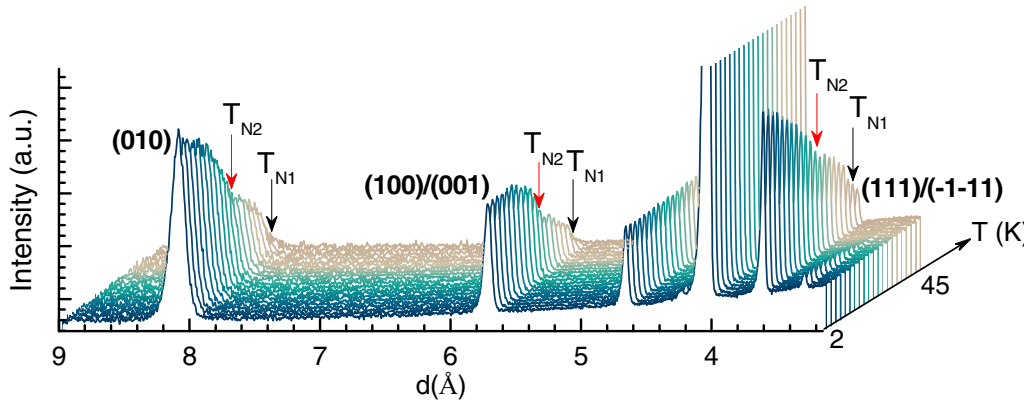

FIG. 7. Thermal evolution of magnetic reflections below T_{N1}. The plotted temperature range is 2–45 K. The black arrows indicate the onset of the magnetic Bragg reflections T_{N1} and the red arrows highlight the changes in the diffracted intensity at T_{N2}. A small but clear enhancement in diffracted intensity below T_{N2} (red arrow) is evident in the graph.

clearly supports the presence of two magnetic transitions. It is to be noted that no further deviation or anomalous change in the long-range order parameter (integrated intensity) has been observed at T^* in Sr_2YbRuO_6. A similar two-step behavior (at $T_{N1} = 31.9$ K and at $T_{N2} = 24$ K) in the intensity of the magnetic Bragg peaks was also observed for Sr_2YRuO_6 [3] and has been interpreted as corresponding to a 2D magnetic transition (where only half the Ru planes ordered magnetically) at T_{N1} followed by a 3D magnetic transition (all Ru atoms order magnetically) at T_{N2}. Unfortunately no details on the space group used in the analysis of the magnetic structure of Sr_2YRuO_6 or of the Wyckoff positions of the Ru atoms used during the refinement of the neutron-diffraction data were given. The idea of having only half of the Ru layers magnetically ordered below T_{N1} while all Ru layers become magnetic ordered below T_{N2} demands the existence of two different crystallographic sites for the Ru atoms in the crystal structure of Sr_2YRuO_6. This is not the case in the normally used space group $P2_1/n$ where only one crystallographic Ru site exists.

To investigate the corresponding changes in the magnetic structure of Sr_2YbRuO_6, Rietveld refinements were done using the total diffracted intensities and the temperature-dependent difference data sets where the nuclear contribution using the 45-K data set had been subtracted. The difference data sets are more sensitive to small changes of the magnetic structure expected to happen at T_{N2}. All the five banks of data have been refined simultaneously to get the final parameters. Figure 9 represents the Rietveld refined plot of the 100 K

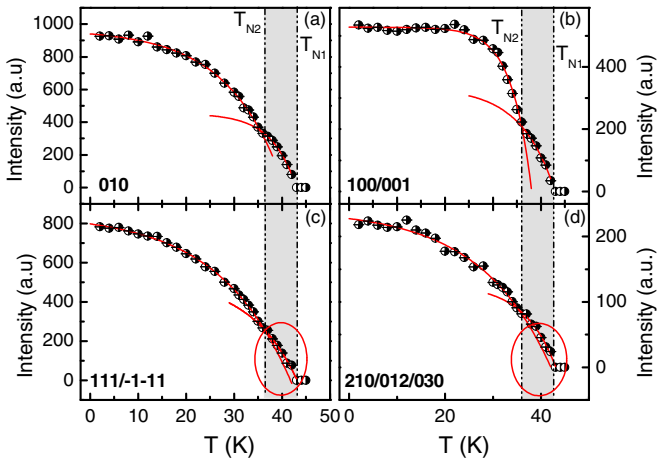

FIG. 8. (a)–(d) The temperature variation of the integrated intensity of various magnetic reflections extracted from the difference curve. Error bars are smaller than the symbol size. Two components are clearly visible as shown by the two red lines and highlighted by the shaded regions. The second component starts growing below T_{N2}. (Refer to the text for details.)

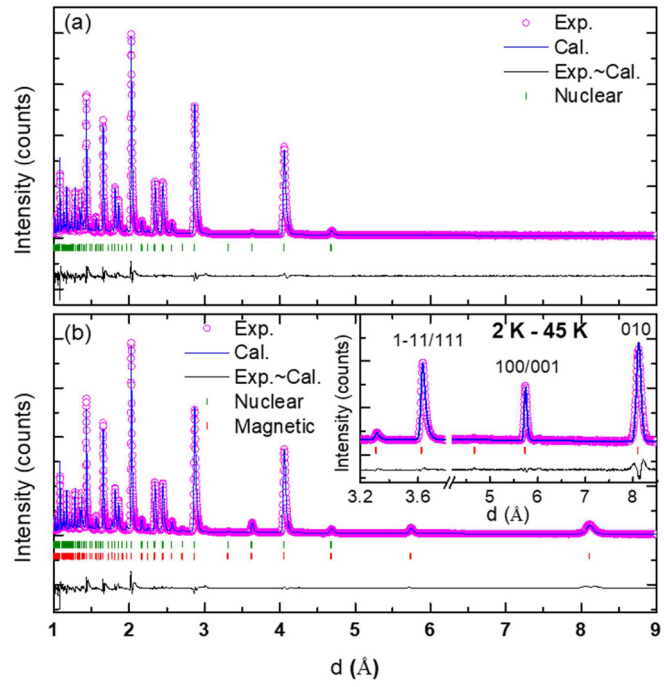

FIG. 9. Rietveld refined NPD patterns collected at (a) 100 and (b) 2 K. Two series of tick marks in (b) correspond to the nuclear (upper, green) and magnetic (lower, red) Bragg reflections. The observed, calculated intensities, and difference are plotted as solid circles, solid line, and bottom line, respectively. The inset in (b) shows the fitted difference data (2–45 K) using just the magnetic model.

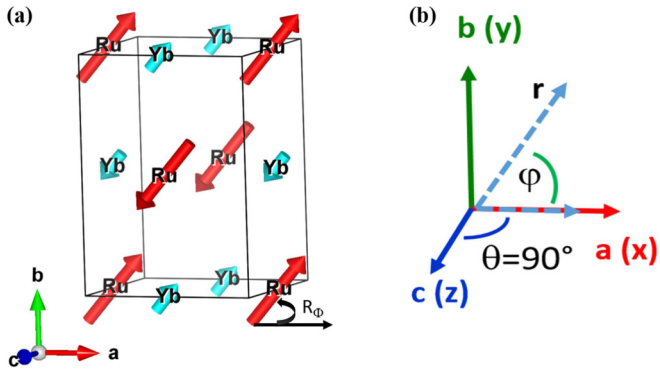

FIG. 10. (a) The magnetic structure of Sr_2YbRuO_6 for $k = (0\,0\,0)$. The Yb^{3+} and Ru^{5+} moments are shown by cyan (small) and red colored (large) arrows, respectively. (b) The spherical coordinate setting used in the present work.

[Fig. 9(a)] and 2-K [Fig. 9(b)] data from the bank 2 of WISH instrument. The 100-K data were fitted with a nuclear phase having the monoclinic space group $P2_1/n$. A very minute (∼1.5 %) impurity of Yb_2O_3, which orders at 2.25 K [19], was found as well in the NPD pattern. The 2 K data are fitted using a two-phase (nuclear + magnetic) model. The inset in Fig. 9(b) shows the Rietveld refined plot of the difference data at (2–45 K) fitted only with the magnetic phase using a fixed scale factor determined from the refinement of the purely nuclear data at $T = 45$ K. The refined lattice parameters at 2 K are $a = 5.7305(2)$ Å, $b = 8.1021(3)$ Å, $c = 5.7360(2)$ Å, and $\gamma = 90.20(2)^\circ$. It should be noted here that we have used the $P112_1/n$ setting instead of the standard $P12_1/n1$ [$a = 5.7314(2)$ Å, $b = 5.7367(1)$ Å, $c = 8.1029(3)$ Å, $\beta = 90.182(1)^\circ$ at 100 K] used in the previous work of Doi *et al.* [15], because the former gives an advantage to adopt the polar coordinates during the refinement procedure. The empirically determined magnetic form factor of Ru^{5+} has been used for the refinement [27]. Magnetic symmetry analysis was performed using the space group $P2_1/n$ with $k = (0, 0, 0)$ using the program BASIREPS [28] which generates two possible irreducible representations (IR1 and IR2), each containing three basis vectors. IR1 has ferro- (F) coupling along the c direction and antiferro- (AF) coupling in the a and b directions while, on the contrary, the IR2 has AF coupling in the c direction and F-coupling in the a and b directions. The best fit of the data can be achieved with a single IR1, having AF coupling along the a and b direction. A collinear model, having parallel Yb^{3+} and Ru^{5+} moments, has been used to refine the data for the magnetic structure determination. Any attempt to avoid this constraint leads to instabilities and divergence of the refinements. The final magnetic structure presented in Fig. 10 consists of an interpenetrating lattice of canted moments of Yb^{3+} and Ru^{5+} ions where FM sheets extending within the a-c plane are coupled antiferromagnetically along the b direction. The spins are pointing along the long b axis with an angle of ∼45–51° (temperature dependent) with respect to the a axis. Figure 10(b) explains the different angles used to describe the magnetic structure. For comparison, we plotted in Fig. S1 of the Supplemental Material the magnetic structure of Sr_2YbRuO_6 in the two different settings, $P112_1/n$ and $P12_1/n$ [29]. Due to the pseudosymmetry present in the sample an equally good fit of the data can be obtained by refining the magnetic structure with AFM b and c components. This magnetic structure, however, would not be compatible with magnetic symmetry analysis. Doi *et al.* [15] have reported similar magnetic structure with Ru and Yb moments at 23° relative to the c axis at 10 K. Due to the pseudosymmetry present and the absence of magnetic symmetry analysis they were not able to specify whether the canting angle is relative to their a or b axis. Sr_2TbRuO_6 [5] and Sr_2YRuO_6 [30] are the only other members of this family of double perovskites for which a spin canting (20°, respectively 10.5° from the long axis) is known [5]. The direction of the magnetic moments of Yb^{3+} and Ru^{5+} is different in the present system from those of the Ho, Tb, and Dy based double ruthenates [5,8,31]. The coupling between the Yb^{3+} and the Ru^{5+} moments is FM whereas an AFM coupling was observed between the rare-earth RE^{3+} and Ru^{5+} for RE = Ho, Tb, Dy, and Tm. While the spins are canted from the long axis in Sr_2YbRuO_6, in Sr_2DyRuO_6 both the Dy and Ru spins are at 90° to the long axis (i.e., in the plane) [8], while in Sr_2TmRuO_6 both the Tm and Ru spins are strictly pointing along the long axis [15]. The values of the Yb^{3+} and the Ru^{5+} moments at 2 K, obtained in this work, are $\mu_{Yb3+} = 0.54(1)\,\mu_B$ and $\mu_{Ru5+} = 2.10(1)\,\mu_B$. The strong reduction of μ_{Yb3+} compared to the expected value of ∼4.5 μ_B matches with similar discrepancies observed for rare-earths' moment for the other members of Ru-based perovskites family, like Sr_2DyRuO_6, Sr_2HoRuO_6, and Sr_2TbRuO_6, etc. [5,8,15,31]. A reduced RE moment is frequently assigned to the effect of the crystal field on the rare-earth cation and/or due to the nondeveloped RE-RE direct magnetic exchange.

Magnetic symmetry analysis allows a FM component in IR1 on the Yb^{3+} and the Ru^{5+} moments along the c direction. The expected FM contribution to the magnetic Bragg peaks comes, however, on top of the nuclear peaks. The intensity of the nuclear peaks is determined by the atom coordinates, the B factor (thermal factor), etc., which can all change slightly with temperature. Our attempt to determine the FM component gave very large errors and the results were not reliable. This is not surprising as the FM component of the moments expected from the magnetization isotherm measurements at 5 K given in Fig. 2(b) is very small ∼0.01 μ_B. Table I contains the information on the bond lengths and bond angles variation during these transitions. No sudden change or variation in the bond lengths/bond angles was noticed at T_{N2} or T^*.

To discern the changes of the magnetic structure at T_{N2}, the temperature variation of the magnetic moments has been determined by Rietveld refinement of the temperature-dependent difference data sets. The refined Ru^{5+} and Yb^{3+} moments are plotted in Fig. 11 as a function of temperature alongside the angle R_Φ, which describes the canting of the moments with respect to the x axis (a axis), and the normalized moments. The value of R_θ was kept constant and equal to 90° [see Fig. 10(b) for the definition] reflecting the nonexistence of an FM component along the c direction. There are small but clear anomalies in the temperature dependence of the moments (more pronounced for Yb^{3+}) and in the R_Φ value at T_{N2}. The Yb^{3+} moments show a sharp increase (similar to the Ru^{5+} moments) below T_{N1}, but show an arrest in the

TABLE I. Selected bond angles (deg) and bond lengths (Å) in paramagnetic (45 K) and AFM state (2 K) of Sr_2YbRuO_6.

Bond angles (deg)	45 K	2 K	Bond lengths (Å)	45 K	2 K
O1-Ru-O2	90.2(4)	90.1(4)	Ru-O1	1.958(8)	1.960(9)
O1-Ru-O3	90.9(4)	90.8(4)	Ru-O2	1.959(9)	1.957(1)
O2-Ru-O3	89.5(3)	89.2(4)	Ru-O3	1.941(8)	1.944(8)
O1-Yb-O2	87.9(4)	91.9(4)	Yb-O1	2.164(8)	2.163(9)
O1-Yb-O3	90.1(3)	89.8(3)	Yb-O2	2.172(9)	2.172(1)
O2-Yb-O3	89.1(3)	89.3(3)	Yb-O3	2.182(8)	2.180(8)
Ru-O1-Yb	159.1(5)	159.0(5)	Ru-Ru	5.737(3)	5.731(4)
Ru-O2-Yb	157.7(5)	158.1(5)	Ru-Yb	4.054(1)	4.045(1)
Ru-O3-Yb	158.4(5)	158.1(5)	Yb-Yb	5.736(4)	5.736(4)

slope near T_{N2}, before it is increasing again more strongly (almost linearly with temperature) and saturating near 10 K. The angle R_Φ which is determined by the relative sizes of the two AFM components along the a and the b directions also shows a continuous increase down to T_{N2}, below which it slightly decreases before saturating to ∼50°. Also, from Fig. 11(d), it appears that below T_{N2} the Ru^{5+} moments attain the saturation value with a much faster rate compared to Yb^{3+}. Noticeably, the rate of increase of the Ru^{5+} and Yb^{3+} moments is different only below T_{N2} while both the moments increase with the same rate between T_{N1} and T_{N2}. Resuming the analysis of the temperature dependent refinement of the difference data sets one can say that a broad but clear peak in R_Φ along with a small plateau in the size of the Yb^{3+} moments appear near T_{N2}. The change in the temperature variation of the normalized moments further confirms the change of the magnetic interactions leading to the magnetic structure at T_{N2} in Sr_2YbRuO_6. In this context, it has to be noted that we have not seen any sign of elastic diffuse scattering between T_{N1} and T_{N2} in our WISH diffraction data of Sr_2YbRuO_6. This is different from the behavior observed in

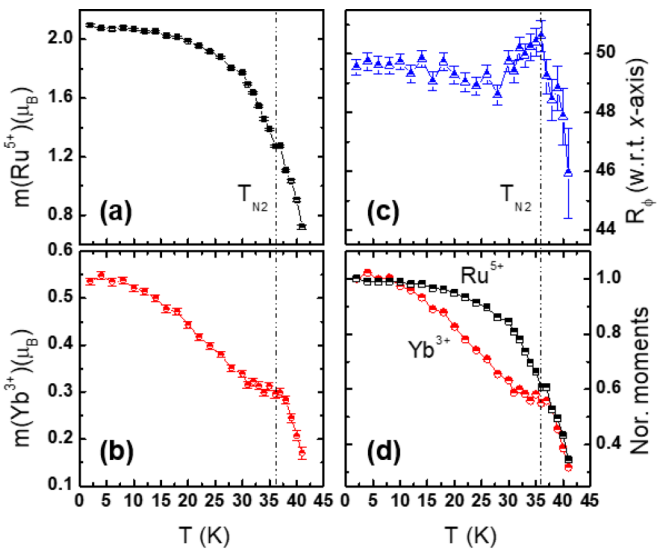

FIG. 11. Thermal variation of (a) Ru^{5+} moments, (b) Yb^{3+} moments, (c) moments angle R_ϕ [with respect to (w.r.t.) x axis/a axis] while $R_\theta = 90°$, and (d) the normalized moments of Yb^{3+} and Ru^{5+}. The vertical black dashed line corresponds to T_{N2}.

Sr_2YRuO_6 [3] and in the cubic Ba_2YRuO_6 [13] where the presence of short-range spin correlations has been observed between T_{N1} and T_{N2} and connected to a two-dimensional (2D) ordering and the absence of true long-range magnetic order. Differences between the RE = Y and Yb compounds could be linked to the different levels of magnetic frustration present in the Sr_2RERuO_6 (RE = rare-earths) compounds. Using the frustration index $f = |\theta_{CW}|/T_N$ [32] to quantify the frustration, values of f ranging from 0.5 to 0.7 for Gd to Er, increasing to 1.3 for Tm, 5.35 for Yb, 9.1 to 11.2 for Y, and 11.7 for Lu can be found (Table II). High values of f have also been observed in Ba_2RERuO_6, 17 for RE = Y and 18 for RE = Lu (see Table II). This gives some indication that the magnetic frustration in Sr_2YbRuO_6 (Ba_2YbRuO_6) is reduced compared to Sr_2YRuO_6 (Ba_2YRuO_6) and could explain why the ordering at T_{N1} is three dimensional.

The size of the Ru^{5+} moment determined for Sr_2YbRuO_6 is very similar to the reported values for other members of this double-perovskite family and points to the fact that in these systems the Ru-O-O-Ru interactions are the strongest magnetic interactions, which control the Ru ordering [3,5,8,15,32]. The very low value of $T_N = 2.3$ K for the rare-earth oxide Yb_2O_3 indicates that Yb-O-Yb interactions are in general very weak [19]. For the well-ordered double-perovskite Sr_2YbRuO_6, even weaker supersuperexchange Yb-O-O-Yb interactions will be present. The absence of magnetic order down to 2 K in Sr_2YbMO_6 (M = Nb, Ta, and Sb) [33] indicates as well that Yb-Yb interactions are weak in these double perovskites. These interactions cannot be responsible for the Yb^{3+} ordering at T_{N1}. Therefore, it appears that the Ru-O-Yb interactions have an important role in governing the magnetic ordering of the rare-earth cation Yb^{3+}. Noticeably, the Yb^{3+} moment exhibits deviation from the mean-field-type behavior as a function of temperature while the Ru^{5+} moment follows the mean-field-type behavior down to 2 K. This indicates that in the rare-earth and ruthenium-based perovskites, the primary magnetic ordering below T_{N1} is induced by the order of the 4d electrons of Ru^{5+} rather than by that of the rare-earth cation, as is also verified for Sr_2RERuO_6 (RE = Ho, Tb, and Dy) [5,8].

IV. THEORETICAL DISCUSSION

To explain the properties of Sr_2YbRuO_6 it is necessary to discuss the microscopic contributions determining the magnetic properties. As mentioned above, the most important one

TABLE II. (a) Sr_2RERuO_6: The reported values of Weiss constant (θ_{CW}), T_N, and the corresponding value of frustration index $f = |\theta_{CW}|/T_N$. (b) Ba_2RERuO_6: The reported values of Weiss constant, T_N, and the corresponding value of frustration index.

(a) Rare earth (RE)	θ_{CW} (K)	T_N (K)	$f = \theta_{CW}/T_N$	References
Gd	−8.0	15.3	0.5	[41]
Tb	−20	41	0.4	[31]
Dy	−25	39.5, 36.5	0.7	[8]
Ho	−20	20[a], 36	0.6	[42]
Er	−15.4	36	0.5	[43]
Tm	−47	36	1.3	[15]
Yb	−225	36, 42	5.35	[15]
Lu	−353	30	11.7	[6]
		27.2[b], 29[b]		[43]
Y	−292	25, 32	9.1	[44]
Y	−273.54	26,30	9.8	[38]
Y	−336.6	24, 30	11.22	[45]
(b) Rare earth (RE)	θ_{CW}	T_N	$f = \theta_{CW}/T_N$	References
La	−383	29.5	13	[46]
Pr	−133	117	1.14	[47]
Nd	−35.5	27[c], 58[c]	0.61	[32]
Ho	−19.9	22, 50	0.398	[48]
Er	−14.6	40	0.365	[49]
Tm	−34	42	0.81	[15]
Yb	−181	48	3.78	[15]
Lu	−630	35	18	[6]
Y	−630	37	17	[6]
	−522	37[d],46[d]	16	[50]

[a]For zero-field-cooled peak in the susceptibility.
[b]Two transitions in the heat capacity.
[c]Two transitions in the magnetic susceptibility, but the heat capacity shows only one peak at 58 K.
[d]Two transition in the magnetic susceptibility, but heat capacity shows only one peak at 36 K.

is the Ru-Ru exchange interaction. For the t_{2g}^3 occupation of Ru^{5+} ions it is relatively straightforward to understand: there are no orbital degrees of freedom and the exchange is the same for nearest neighbors in all directions. Simple arguments, illustrated in Fig. 12(a), demonstrate that the Ru-O-O-Ru nearest-neighbor (NN) exchange is AFM, in accordance with the Goodenough-Kanamori-Anderson (GKA) rules [34–36]; see, e.g., the discussion in [37]. Because of the t_{2g}^3 occupation, the AFM exchange would be the same for NN in xz and in yz planes. With AF interaction to 12 nearest-neighbor Ru's one stabilizes the type-I magnetic structure (FM planes stacked antiferromagnetically): one has in this case eight NN AFM pairs and only four NN FM ones.

Similar arguments also explain the exchange between Ru and Yb; as indicated above, the direct Yb-Yb exchange is definitely much smaller and can play a role only at very low temperatures. The ground state of Yb^{3+} ($4f^{13}$) in this case is the Γ_6 doublet [31]; the shape of its wave function is sketched in Fig. 12(b) from Ref. [38]. One sees that the occupied t_{2g} orbitals of Ru are orthogonal to the Γ_6 states of Yb, i.e., the only exchange processes could be due to the virtual hopping from occupied to empty states, which, according to GKA rules, gives FM Yb-Ru coupling. This naturally explains why

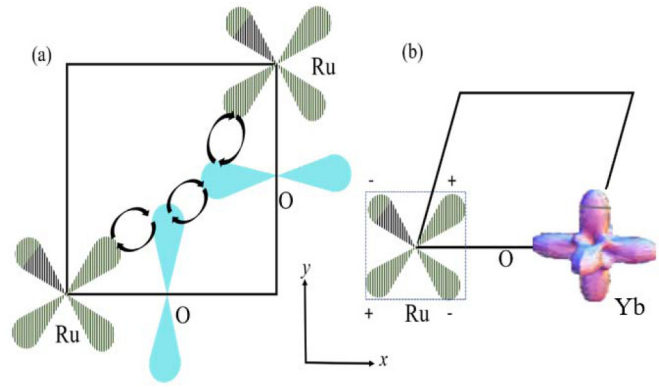

FIG. 12. The schematic orbital diagrams of Ru^{5+}, O^{2-}, and Yb^{3+}. (a) Mechanism of AFM Ru-Ru exchange. Grey are Ru t_{2g} orbitals, blue are O $2p$ orbitals and (b) schematic illustration of FM Ru-Yb exchange interaction. Grey is Ru t_{2g} orbital and purple is Yb Γ_6 (CEF ground state) orbital taken from Ref. [34].

Yb spins are ordered parallel to the spins of ferromagnetically ordered Ru planes. Combining the Ru-O-O-Ru exchange and the Ru-Yb coupling one gets indeed exactly the magnetic structure observed in Sr_2YbRuO_6: type-I ordering of both Ru and Yb sublattices being parallel, i.e., ferromagnetically coupled.

One of the interesting and important questions is the nature of two magnetic transitions in many ruthenium double perovskites, including Sr_2YbRuO_6. As one can see from Table II, more than half (five of nine) of the known Sr_2RERuO_6 systems have a double transition. Sometimes it is seen in the magnetic data, sometimes in the specific heat, sometimes in both. Apparently, there is no (strong) change of the lattice at these transitions, i.e., they are of predominantly magnetic origin (although some effect on the lattice cannot be excluded, for example due to magnetostriction). Interestingly, these two transitions are seen both for magnetic REs (Dy, Ho, Yb) and for nonmagnetic ones (Lu, Y). From this we can conclude that it is predominantly the Ru subsystem which is responsible for the two transitions.

Based on experimental data there are two factors invoked, which could be responsible for the existence of two transitions. As already mentioned above, one explanation was put forward by Granado *et al.* in Ref. [3]: In this paper based on neutron scattering it was concluded that in Sr_2YRuO_6 there appears two-dimensional ordering at T_{N1}, which becomes three dimensional below T_{N2}. The indication for this behavior was the presence of strong diffuse neutron scattering between T_{N1} and T_{N2}, which the authors attributed to the absence of full 3D ordering in this temperature range, i.e., between T_{N1} and T_{N2}. However, we observe no such elastic diffuse scattering and as such this explanation does not apply to our system.

The other effect noticed in Sr_2YRuO_6 by Singh *et al.* [2] and by Kayser *et al.* [30], which is also seen in our data, see Fig. 11(c), is the slight change of the spin direction at T_{N2}. This could be another reason for the second transition: it could be predominantly a spin reorientation. We have to point out here that our use of the term "spin reorientation" has to be understood as a nonmonotonic change of the spin structure within the same irreducible representation. There is neither a

change of the crystallographic nor of the magnetic symmetry connected to T_{N2}. The data of Fig. 11(c) show this change of the spin orientation in approaching T_{N2}. The behavior of the magnetization in the ZFC and especially in the FC regime shown in Fig. 2(a), with spin compensation, also corroborates this explanation. As such behavior is seen in both Y and Yb systems, it is hardly connected to the direct influence of the rare-earths (although the details may depend on those). Most probably, it is related to the specific characteristics of the Ru ions, namely to its single-site anisotropy and to the Dzyaloshinskii-Moriya (DM) interaction existing in the crystal structure of Sr_2YbRuO_6. In this sense the situation here strongly resembles that found in YVO_3 [39,40] in which a compensation point was also seen in a system with only one type of magnetic ions (whereas the most common reason for compensation points is the interplay of two magnetic sublattices with different ions, having different magnetic moments). Such behavior in YVO_3 was explained in [39,40] as an interplay of two mechanisms of magnetic anisotropy: single-site anisotropy KS_z^2 and DM interaction. Both mechanisms can create magnetization, which, however, can point in opposite directions, with different mechanisms dominating in different temperature intervals, which can lead to spin compensation at some temperature. We suppose that the same mechanism may operate also in Sr_2YbRuO_6 and could lead to both spin compensation and the appearance of the spin reorientation transition. This mechanism relies on a "fine tuning" of two mechanisms determining the spin direction, and the resulting behavior may depend on the details of the system. As the magnetic anisotropy of a magnetic RE will probably contribute as well to the total balance, this can explain why the double transitions are seen in some materials, for some RE ions, but not in the others. We have used a point-charge model of the crystal field to calculate the single-ion anisotropy of the Yb ion in Sr_2YbRuO_6, which shows that the easy axis of the magnetization is the *b* axis (i.e., along the long axis).

Thus, on the basis of the results of our experiments, and also analyzing the tendencies in this whole class of materials, we suggest that the main mechanism governing the second magnetic transition in these systems is connected to details of the magnetic anisotropy of the Ru and the RE system and their temperature dependence. But the real proof of this picture may require additional studies on single crystals.

V. CONCLUSIONS

We have investigated the ordered double-perovskite Sr_2YbRuO_6 using various experimental techniques to understand the origin of two magnetic transitions. The bulk magnetization measurements of Sr_2YbRuO_6 reveal the presence of two clear magnetic transitions as a function of temperature, namely at $T_{N1} = 42$ K, at $T_{N2} = 36$ K, and a very weak anomaly at $T^* = 10$ K. The heat capacity measurements reveal a clear signature of T_{N1} and T_{N2} indicating the long-range ordering whereas no anomaly can be detected at T^*. Our detailed μSR and NPD results provide a concrete evidence of long-range magnetic ordering of both sublattices (Ru^{5+} and Yb^{3+}) below T_{N1} and a clear change in the long-range magnetic ordering parameters at T_{N2}. The magnetic ordering is primarily controlled by the Ru^{5+} moments, but a change in the spin structure at T_{N2} is confirmed based on the temperature variation of Yb^{3+} and Ru^{5+} moments and of the angle R_ϕ describing the moment direction. All the observed magnetic Bragg peaks can be indexed with a single propagation vector $\boldsymbol{k} = (0, 0, 0)$ and the magnetic structure consists of interpenetrating sublattices of Yb^{3+} and Ru^{5+} spins having confined moments in the *ab* plane. The resultant magnetic structure is composed of parallel spins of Yb^{3+} and Ru^{5+} having an angle of $R_\phi \sim 45$-51° with respect to the *a* direction.

Based on our and related data on similar systems, we propose that the second magnetic transition and the presence of a compensation point in the magnetization observed in many materials of this class may be related to details of anisotropic mechanisms (single ion and Dzyaloshinskii-Moriya) acting mainly in the Ru subsystem with RE ions playing a possible but not necessary role. It has been shown that a change of the details of the spin structure of the two sublattices ordering concomitantly at T_{N1} is present between T_{N1} and T_{N2}. This finding can be added to the formerly proposed mechanisms of separate order of the two magnetic sublattices or of a change between 2D and 3D magnetic order. The present results should therefore be useful to develop realistic theoretical models to explain the presence and the mechanisms of two magnetic transitions in this double perovskite family. As seen on the example of the present study on Sr_2YbRuO_6, a prerogative for advancing further would demand better temperature-dependent bulk measurements and neutron data on single crystals.

ACKNOWLEDGMENTS

S.S. would like to acknowledge the Nanomission project of the Department of Science and Technology, India, for providing a postdoctoral fellowship during this work. D.T.A. and A.D.H. would like to acknowledge financial assistance from CMPC-STFC Grant No. CMPC-0910. The work of D.I.K. was funded by the Deutsche Forschungsgemeinschaft (DFG, German Research Foundation), Project No. 277146847-CRC 1238. We would like to thank C. V. Tomy, R. Singh, and W. Kockelmann for participating in the initial stage of this project on GEM and R. Singh for providing the sample. We thank F. Orlandi for his help during the WISH experiment and R. Stewart, G. Nilsen, and A. Amorese for interesting discussions.

[1] P. L. Bernardo, L. Ghivelder, H. S. Amorim, J. J. Neumeier, and S. Garcia, New J. Phys. **17**, 103007 (2015).

[2] R. P. Singh and C. V. Tomy, Phys. Rev. B **78**, 024432 (2008).

[3] E. Granado, J. W. Lynn, R. F. Jardim, and M. S. Torikachvili, Phys. Rev. Lett. **110**, 017202 (2013).

[4] R. P. Singh and C V Tomy, J. Phys.: Condens. Matter **20**, 235209 (2008).

[5] N. G. Parkinson, P. D. Hatton, J. A. K. Howard, C. Ritter, R. M. Ibberson, and M.- K. Wu, J. Phys.: Condens. Matter **16**, 7611 (2004).

[6] P. D. Battle and C. W. Jones, J. Solid State Chem. **78**, 108 (1989).

[7] A. A. Aczel, P. J. Baker, D. E. Bugaris, J. Yeon, H.-C. zur Loye, T. Guidi, and D. T. Adroja, Phys. Rev. Lett. **112**, 117603 (2014).

[8] D. T. Adroja, S. Sharma, C. Ritter, A. D. Hillier, D. Le, C. V Tomy, R. Singh, R. I. Smith, M. Koza, A. Sundaresan, and S. Langridge, Phys. Rev. B **101**, 094413 (2020).

[9] A. P. Mackenzie and Y. Maeno, Rev. Mod. Phys. **75**, 657 (2003).

[10] J. M. Longo, P. M. Raccah, and J. B. Goodenough, J. Appl. Phys. **39**, 1327 (1968).

[11] C. I. Hiley, M. R. Lees, J. M. Fisher, D. Thompsett, S. Agrestini, R. I. Smith, and R. I. Walton, Angew. Chem. Int. Ed. Engl. **53**, 4423 (2014).

[12] R. Greatrex, N. N. Greenwood, M. Lal, and I. Fernandez, J. Solid State Chem. **30**, 137 (1979).

[13] G. J. Nilsen, C. M. Thompson, G. Ehlers, C. A. Marjerrison, and J. E. Greedan, Phys. Rev. B **91**, 054415 (2015).

[14] Y. Doi and Y. Hinatsu, J. Phys.: Condens. Matter **11**, 4813 (1999).

[15] Y. Doi, Y. Hinatsu, A. Nakamura, Y. Ishii, and Y. Morii, J. Mater. Chem. **13**, 1758 (2003).

[16] R. P. Singh, C. V Tomy, and A. K. Grover, Appl. Phys. Lett. **97**, 182505 (2010).

[17] L. C. Chapon, P. Manuel, P. G. Radaelli, C. Benson, L. Perrott, S. Ansell, N. J. Rhodes, D. Raspino, D. Duxbury, E. Spill, and J. Norris, Neutron News **22**, 22 (2011).

[18] J. Rodríguez-Carvajal, Phys. B: Condens. Matter **192**, 55 (1993).

[19] R. M. Moon, H. R. Child, W. C. Koehler, and L. J. Raubenheimer, J. Appl. Phys. **38**, 1383 (1967).

[20] M. Costes, J. M. Broto, B. Raquet, H. Rakoto, M. A. Novak, J. P. Sinnecker, S. Soriano, W. S. D. Folly, A. Maignan, and V. Hardy, J. Magn. Magn. Mater. **294**, e123 (2005).

[21] E. Lefrançois, L. C. Chapon, V. Simonet, P. Lejay, D. Khalyavin, S. Rayaprol, E. V Sampathkumaran, R. Ballou, and D. T. Adroja, Phys. Rev. B **90**, 014408 (2014).

[22] P. Yadav, S. Sharma, P. J. Baker, P. K. Biswas, I. da Silva, R. Raghunathan, U. Deshpande, R. J. Choudhary, N. P. Lalla, and A. Banerjee, Phys. Rev. B **99**, 214421 (2019).

[23] S. Sharma, P. Yadav, T. Sau, P. Yanda, P. J. Baker, I. da Silva, A. Sundaresan, and N. P. Lalla, J. Magn. Magn. Mater. **492**, 165671 (2019).

[24] A. A. Aczel, Z. Zhao, S. Calder, D. T. Adroja, P. J. Baker, and J.-Q. Yan, Phys. Rev. B **93**, 214407 (2016).

[25] C. R. Wiebe, J. E. Greedan, P. P. Kyriakou, G. M. Luke, J. S. Gardner, A. Fukaya, I. M. Gat-Malureanu, P. L. Russo, A. T. Savici, and Y. J. Uemura, Phys. Rev. B **68**, 134410 (2003).

[26] J. Sannigrahi, D. T. Adroja, C. Ritter, W. Kockelmann, A. D. Hillier, K. S. Knight, A. T. Boothroyd, M. Wakeshima, Y. Hinatsu, J. F. W. Mosselmans, and S. Ramos, Phys. Rev. B **99**, 184440 (2019).

[27] N. G. Parkinson, P. D. Hatton, J. A. K. Howard, C. Ritter, F. Z. Chien, and M.-K. Wu, J. Mater. Chem. **13**, 1468 (2003).

[28] C. Ritter, Solid State Phenom. **170**, 263 (2011).

[29] See Supplemental Material at http://link.aps.org/supplemental/10.1103/PhysRevB.102.134412 for comparison of the magnetic structure in two different settings $P12_1/n1$ and $P112_1/n$ of the space group $P2_1/n$.

[30] P. Kayser, B. Ranjbar, B. J. Kennedy, and M. Avdeev, J. Solid State Chem. **249**, 154 (2017).

[31] Y. Doi, Y. Hinatsu, K. Oikawa, Y. Shimojo, and Y. Morii, J. Mater. Chem. **10**, 1731 (2000).

[32] Y. Izumiyama, Y. Doi, M. Wakeshima, Y. Hinatsu, K. Oikawa, Y. Shimojo, and Y. Morii, J. Mater. Chem. **10**, 2364 (2000).

[33] F. C. Coomer, J. Campbell, N. Giordano, O. M. Collins, and E. J. Cussen, J. Solid State Chem. **221**, 411 (2015).

[34] P. W. Anderson, Phys. Rev. **115**, 2 (1959).

[35] J. B. Goodenough, Phys. Rev. **100**, 564 (1955).

[36] J. Kanamori, J. Phys. Chem. Solids **10**, 87 (1959).

[37] D. I. Komsikii, *Transition Metal Compounds* (Cambridge University Press, Cambridge, UK, 2014).

[38] T. Willers, J. C. Cezar, N. B. Brookes, Z. Hu, F. Strigari, P. Körner, N. Hollmann, D. Schmitz, A. Bianchi, Z. Fisk, A. Tanaka, L. H. Tjeng, and A. Severing, Phys. Rev. Lett. **107**, 236402 (2011).

[39] Y. Ren, T. T. M. Palstra, D. I. Khomskii, E. Pellegrin, A. A. Nugroho, A. A. Menovsky, and G. A. Sawatzky, Nature (London) **396**, 441 (1998).

[40] Y. Ren, T. T. M. Palstra, D. I. Khomskii, A. A. Nugroho, A. A. Menovsky, and G. A. Sawatzky, Phys. Rev. B **62**, 6577 (2000).

[41] L. T. Corredor, D. A. L. Téllez, J. L. P. Jr, P. Pureur, and J. Roa-Rojas, J. Mod. Phys. **2**, 154 (2011).

[42] Y. Doi, Y. Hinatsu, K. Oikawa, Y. Shimojo, and Y. Morii, J. Mater. Chem. **10**, 797 (2000).

[43] R. Sáez-Puche, E. Climent-Pascual, R. Ruiz-Bustos, M. A. Alario-Franco, and M. T. Fernández-Díaz, Prog. Solid State Chem. **35**, 211 (2007).

[44] E. B. Guedes, M. Abbate, F. Abud, R. F. Jardim, F. C. Vicentin, and R. J. O. Mossanek, Phys. Rev. B **94**, 045109 (2016).

[45] D. T. Adroja, R. Singh, and C. V. Tomy (unpublished).

[46] P. D. Battle, J. B. Goodenough, and R. Price, J. Solid State Chem. **46**, 234 (1983).

[47] Y. Izumiyama, Y. Doi, M. Wakeshima, Y. Hinatsu, Y. Shimojo, and Y. Morii, J. Phys.: Condens. Matter **13**, 1303 (2001).

[48] Y. Hinatsu, Y. Izumiyama, Y. Doi, A. Alemi, M. Wakeshima, A. Nakamura, and Y. Morii, J. Solid State Chem. **177**, 38 (2004).

[49] Y. Izumiyama, Y. Doi, M. Wakeshima, Y. Hinatsu, A. Nakamura, and Y. Ishii, J. Solid State Chem. **169**, 125 (2002).

[50] T. Aharen, J. E. Greedan, F. Ning, T. Imai, V. Michaelis, S. Kroeker, H. Zhou, C. R. Wiebe, and L. M. D. Cranswick, Phys. Rev. B **80**, 134423 (2009).